ANL/CP--73988

DE91 017989

SEISMIC BASE ISOLATION: ELASTOMER CHARACTERIZATION, BEARING MODELING AND SYSTEM RESPONSE

R.F. Kulak, C.Y. Wang, T.H. Hughes (ANL - USA)

This paper discusses several major aspects of seismic base isolation systems that employ laminated elastomer bearings. Elastomer constitutive models currently being used to represent the nonlinear elastic and hysteretic behavior are discussed. Some aspects of mechanical characterization testing of elastomers is presented along with representative tests results. The development of a finite element based mesh generator for laminated elastomer bearings is presented. Recent advances in the simulation of base isolated structures to earthquake motions are presented along with a sample problem.

Introduction

Seismic base isolation is accepted by civil engineers as a viable strategy for protecting structures from earthquake damage. The main benefits are: (1) the elimination of damage to the civil structure, (2) the reduction in damage to contents and loss time, and (3) the ability to save lives. In contrast, the traditional methods for seismic design (i.e. seismic hardening) may leave the structure standing. However, the internal contents may be severely damaged and the occupants may be subjected to injuries or loss of life. The traditional approach may lead to a long loss of time and costly repairs.

On a worldwide basis, the use of seismic base isolation has been increasing rapidly for such critical facilities as computer centers, medical centers, and emergency control facilities. The Western United States has several buildings that employ seismic isolators. On a global domain, Japan has been the most aggressive in adapting isolation to their structures. Now, more than fifty buildings use or plan to use seismic isolation. Currently there are two French designed nuclear power plants; one is located in Cruas-Meysee, France and the other in Koeberg, South Africa.

From the various devices proposed for seismic isolators, the laminated elastomer bearing is emerging as the preferred device for large buildings/structures (i.e., no more than eight stories in height). The laminated bearing is constructed from alternating thin layers of elastomer and metallic plates (shims). The elastomer is usually a carbon filled natural rubber that exhibits damping when subjected to shear. Recently, some blends of natural and synthetic rubbers have appeared.

This paper reports on several major aspects of seismic base isolation. The first part of this paper looks at several constitutive models that are available for modelling the nonlinear elastic and hysteretic behavior of the elastomer. Next several definitions for shear stiffness and damping ratio are examined. This is followed by a discussion of mechanical characterization testing of the elastomer. Before candidate elastomers can be used in seismic isolation bearings, their response to design-range loads and beyond design-range loads must be determined. Specimen testing should be divided into two categories. In the first category, measurements of the mechanical properties that are specified in the Technical Specifications are made. Thus, this class of testing is for quality assurance of the elastomer produced by the rubber compounder. The second category of tests are performed to determine the response of the elastomer under earthquake-type loading conditions.

Next, the development of a laminated isolation bearing mesh generator for the NEPTUNE finite element code system[1] is presented. The generator provides an efficient tool for developing complex three-dimensional finite element models that include representations for the metallic shims, elastomer layers, and cover layers. Finally, the element formulations and solution strategies used in the simulations are presented.

The final aspect presented here is the simulation of base-isolated structures with elastomeric bearings to earthquake motions. To simulate the bearing behavior, a nonlinear viscoelastic constitutive model is utilized in a special bearing element. The characteristic behavior of the isolation bearing, such as the variation of shear modulus and material damping with the change of maximum shear deformation are captured quite closely by the formulation. Since structural response also depends significantly on the input acceleration time histories acting at the foundation level, a soil analysis is performed to evaluate the foundation input motion as well as the stiffness and damping of the soil deposits. The special bearing element and soil-analysis capability have been incorporated into a three-dimensional system response program, SISEC[2,3] developed at Argonne National Laboratory. Validations of code predictions with experimental and actual earthquake observation data are presented. Moreover, relative responses of isolated and nonisolated structures are investigated. Results show that by using the base-isolation system, the spectra acceleration transmitted to the superstructure is reduced significantly for frequencies between 1.0 and 5.0 Hz.

Constitutive Models

The constitutive model used to represent the elastomer in the bearing is perhaps the most important ingredient to a successful analysis. Bearing elastomers are typically nonlinear hysteretic materials. However, for preliminary studies it is often economical to perform nonlinear elastic analysis. Most currently used finite element programs use a strain-energy function, W, based upon Mooney-Rivilin[4] and Blatz-Ko[5] formulations. For example, the compressible form for the Mooney-Rivilin model is given by

$$W = K_1(J_1 - 3) + K_2(J_2 - 3) + 1/2\ \kappa\ (J_3 - 1)^2 \qquad (1)$$

where J_1, J_2 and J_3 are modified stretch invariants and κ is the bulk modulus. The above forms of the strain-energy function are derived on the basis of uniaxial and biaxial tests. Also, it is known that they are only valid for stretch ratios in the range of 1.1 to 2.2. Thus, the use of these forms beyond the design range is questionable. The laminated elastomeric bearing will be subjected to a combination of compressive and shear forces during a seismic event. Research by van den Bogert and de Borst[6] indicate that the Mooney-Rivilin model does not match experimental data for compression-shear loading. Better compression shear response can be obtained when an Ogden model[7] is employed. The Ogden model is formulated in terms of principal stretches, that is

$$W = \sum_r \frac{\mu_r}{\alpha_r}\left[\lambda_1^{\alpha_r} + \lambda_2^{\alpha_r} + \lambda_3^{\alpha_r} - 3\right] \qquad (2)$$

where λ_i are the principal stretches and μ_r and α_r are constitutive constants that must be determined from experimental data.

Several constitutive models have been proposed to simulate the behavior of elastomeric materials. Koh and Kelly[8] use a fractional derivative representation, and Simo and Taylor[9] use a viscoelastic model with damage effects. In the Simo-Taylor model, the deviatoric viscoelastic stress tensor, S_{ij}, is given by

$$S_{ij} = \int_{-\infty}^{t_n} [G_\infty + (G_o - G_\infty)e^{-(t-s)/\nu}]\, \dot{\pi}_{ij}(s)ds \qquad (3)$$

where K is the bulk modulus, J the determinant of the deformation gradient, δ_{ij} the identity tensor, G_∞ and G_o the long term and short term shear moduli, respectively, t is the time, and ν is the relaxation time constant. The strain history function is expressed by

$$\pi_{ij}(s) = \left[\beta - (1-\beta)\,\frac{1-e^{\psi_s/\alpha}}{\psi_s/\alpha}\right] \text{dev}\, \bar{C}_{ij}(s) \qquad (4)$$

where α and β are material parameters, ψ is the damage parameter, and $\bar{C}_{ij}$ is the volume preserving right Cauchy strain tensor. Equations 1 and 2 identify six material parameters that must be obtained from specimen tests, namely: K, G_o, G_∞, α, ν, and β.

Shear Stiffness

A key mechanical property that determines the fundamental horizontal frequency of a base isolated system is the shear stiffness of the isolator. Because of the relatively high shear modulus of the steel, it is the shear modulus of the elastomer that determines the shear stiffness of the bearing. However, there are several different forms being used to define this quantity. One form is the storage modulus, G', which is given by

$$G' = \frac{\tau(\gamma^+_{max}) - \tau(\gamma^-_{max})}{\gamma^+_{max} - \gamma^-_{max}} \tag{5}$$

where γ^+_{max} and γ^-_{max} are the maximum positive and negative shear strains, respectively, that occur during a complete hysteresis loop, and $\tau(\gamma^+_{max})$ is defined to be the shear strain at γ^+_{max}.

Another form that is popular is the so-called effective shear modulus, G_{eff}, given by

$$G_{eff} = \frac{\tau^+_{max} - \tau^-_{max}}{\gamma^+_{max} - \gamma^-_{max}} \tag{6}$$

where τ^+_{max} and τ^-_{max} are the maximum positive and negative shear stress, respectively. Note, for rounded loops, typical at the lower strain levels, Eqs. 5 and 6 give values that can differ by about 12 percent. For pointed tip loops, which occur at higher strains, the values calculated by both equations are nearly the same. Since the value of the stiffness is used in the computation of the damping factor, the choice of the stiffness form will affect

the value of that quantity. Note, the values needed for Eq. 6 can be determined with greater accuracy.

It is necessary that the form chosen for the shear modulus be explicitly spelled out in the technical specifications for the rubber compound. Otherwise, the compounder may take the liberty to choose his definition and produce an elastomer with unacceptable engineering properties.

Damping Ratio

Another quantity used to characterize elastomers is the damping ratio, ζ. Here again there is not a unique method for determining its value from experimental data. For example, a popular formula for the damping ratio is

$$\zeta = \frac{U_D}{4\pi G' \gamma_{max}^2} \; ; \quad U_D = \oint_0^{2\pi/\omega} \tau \dot{\gamma} dt \; ; \quad G' = \frac{\tau(\gamma_{max})}{\gamma_{max}} \tag{7}$$

where U_D is the energy dissipated per cycle (i.e., the area within the hysteresis loop), G' the storage modulus, γ the shear strain, and τ the shear stress. Note, the storage modulus is defined to be the stress at the maximum strain. The above definition is obtained from a linear viscoelastic model and works well for those materials. It also provides reasonable values for elastomers at strain levels below 100 percent, the range where the hysterisis loops are elliptical. However, at higher levels the loops are no longer elliptical and Eq. 7 gives misleading results. To obtain more reasonable values for the damping ratio, the following definition can be used

$$\bar{\zeta} = \frac{U_D}{4\pi U_S} \; ; \quad U_s = \int_o^{\gamma_{max}} \bar{\tau} d\gamma \tag{8}$$

Here $\bar{\tau}$ defines the average value of the hysteresis loop at a fixed strain level. Thus, the $\bar{\tau}$ curve bisects the hysteresis loop and represents a pseudo elastic response curve. It should be noted

that for linear viscoelastic materials, the $\bar{\tau}$ curve approximates the storage modulus line.

Testing Environment

The elastomer testing facility at Argonne National Laboratory is set up for high precision dynamic testing of small coupon specimens. The laboratory contains two Instron universal testing machines of the 8500 series. These machines have digital electronic controls using the latest technology for dynamic testing. Both machines have identical 55 kip load frames and interchangeable load cells and holding fixtures. One of the machines has a 22 kip electro-mechanical actuator for quasistatic testing and the other machine has a 5 kip hydraulic actuator with a 6 gallon-per-minute hydraulic power supply for dynamic testing. Both machines are connected to 386DX computers that can be programmed for test control, data acquisition and data processing.

At present the hydraulic machine is set up to perform shear tests on three bar specimens (Fig. 1) either of a stress relaxation type or cyclic testing up to 375% strain using a 5 mm thick specimen. Frequencies up to 100 Hz can be handled at very low strain levels. Two sample points on the system performance limiting curve would be 5 mm cyclic amplitude at 10 Hz and 40 mm at 1 Hz. A temperature cabinet is available and will be installed so these shear tests can be performed over a temperature range of -100°F to 400°F. Work is currently underway to develop the capability to perform biaxial shear-compression tests. In this case the hydraulic machine will apply the compressive loads and the electronics from the other machine will control an actuator/load cell combination that will apply the shear loading.

Small samples of the elastomer were tested in shear to obtain the mechanical data required to characterize the elastomers and to validate the constitutive model. The PC computer program used to interface with the operator and analyze the data was written specifically for this type of elastomer testing by one of the authors. The test specimens consist of two elastomer pads 5 mm

thick by 25 mm square mounted in the three bar lap configuration. The specimens are fabricated in a mold by bonding the elastomer to the steel bars during vulcanization. The elastomer tested for this paper is a high damping natural rubber compound provided by Oil States Industries of Arlington, Texas. It is identified as their proprietary compound #259-62.

Each test was performed at room temperature at a selected strain and frequency using a sine wave loading for six consecutive cycles. The values of shear modulus, damping, etc. reported here were calculated using the 100 data points from the hysteresis loop of the sixth cycle. Since the three-bar specimens contain two pads, the results represent an average for the two pads. In most elastomer testing, the amount the specimen has been worked before the test can have a marked effect on the results. This will be noted in the discussion of the results since we had some difficulty in obtaining consistent values. Reference to a scragged state usually refers to a prior loading of approximately thirty cycles at 0.5 Hz and the desired strain level or extensive testing within the past hour. Reference to an unscragged state usually indicates a 24 hour rest period.

Test Results

To characterize the elastomer under a variety of conditions, the test specimens were subjected to several types of tests. The test results provide a data base for benchmarking constitutive models and comparing various elastomers.

The first test performed was a prescribed strain test in which the specimen was subjected to six cycles at each strain level. The following strain sequence was prescribed ±5, ±10, ±20, ±50, ±100, ±150, ±200, ±250, and ±300 percent shear strain. Figure 2 shows the variation in stiffness with shear strain at 0.5 Hz. The stiffness reduces in value in the range of 0 to 100 percent and begins to increase in value around 150 percent. The first cycle values were always greater than the sixth cycle. The variation in damping with strain is shown in Fig. 3. The difference in damping

ratio as calculated by Eqs. 5 and 6 is also shown. The rubber specimen tests indicate that the energy dissipation varied with the square of the strain. Figure 4 shows the hysteresis loop for the 300 percent test. The pseudo elastic response curve is shown by the dashed curve and the linear elastic response curve by the dotted line.

The second test performed was an up-down strain sequence test. This test was conducted by subjecting the specimen to a series of increasing strain levels followed by a series of decreasing strain levels. The specimen was subjected to six cycles of an increasing strain sequence (±5, ±10, ±20, ±50, ±100, ±150 percent) immediately followed by six cycles of a decreasing strain sequence (±100, ±50, ±20, ±10, ±5 percent). Table 1 gives the values for stiffness during the increasing strain sequence, decreasing strain sequence, and the average of the two. It was noticed that the stiffness at a specific strain level is always less during the down sequence than during the up sequence. Also, the percent difference is greater at the lower strain levels.

The next test was performed to determine the variation in stiffness and damping with frequency. The specimens were tested at the following frequencies: 0.01, 0.1, 0.5, 0.8, 1, 5, and 10 Hz. The maximum strain at each frequency was limited by the performance envelope of the testing machine. For example, the 5 percent strain tests were performed at all frequencies, and the 150 percent strain tests were performed only up to 1.0 Hz. Figures 5 and 6 show the frequency dependence of the stiffness and damping. It is noted that for the seismic isolation system design frequency range (0.4 to 1.0 Hz), the variations in stiffness and damping are small. Also, these variations indicate that the material damping is close to being hysteretic.

Relaxation tests were performed to determine the elastomer's behavior under constant strain. A shear strain was applied to the specimen and held for 36 seconds. The resulting stress relaxation is shown in Fig. 7. It is seen that the stress drops rapidly from

its initial value. Figure 8 shows the effect that "scragging" has on the relaxation behavior.

Three-Dimensional Finite Element Modeling

The NEPTUNE finite element code system is being enhanced with features needed to treat the unique aspects of a laminated isolation bearing. One of the key areas of development was the enhancement of NEPTUNE's preprocessor code, PRENEP, with a laminated elastomer bearing mesh generator. The mesh generator was designed to automatically generate the nodes and elements for the end plates, shim plates, core rubber and cover layer. The user specifies the dimensions of these components, the number of shim plates, and discretization parameters. The newly-developed generator automatically determines the nodal coordinates and element connectivity. To illustrate, Fig. 9 shows the design drawing for a representative bearing. The bearing is 206 mm high and has an outer diameter of 373 mm. The bearing was designed with 12 layers of 10 mm thick rubber and 11 steel shims. The end plates contain bolt holes for mounting to flange plates that are attached to a basemat and superstructure. Figure 10 shows a partially generated finite element model for the bearing. At this point of the mesh generation process, the entire lower end plate has been generated. In addition, the central portion, which contains alternating layers of rubber and steel and a part of the upper end plate have been generated. Figure 11a shows a single outer layer of rubber that is discretized by three (3) elements through the thickness, and Fig. 11b shows a single outer layer of shim. The entire cover layer is shown in Fig. 12. The completed model is displayed in Fig. 13; it contains 3666 elements and 4464 nodes.

Description of Improved System Response Program, SISEC

As part of the analytical development, a three-dimensional program SISEC (Seismic Isolation System Evaluation Code) is being developed at ANL for calculating the global response of isolators

and isolated structures. The basic code utilizes beam, nonlinear spring and plate elements to model the isolated structure together with an elastic half space approach to evaluate the impedance functions of the soil domain.[1]

Recently significant improvements have been made to the SISEC code.[2,3] First, to closely simulate the bearing behavior, a nonlinear viscoelastic constitutive model by Simo and Taylor[9] has been modified[10] and implemented into the SISEC code. This formulation requires six input parameters derived from sinusoidal experimental data. The characteristic behavior of the isolation bearing, such as the variation of shear modulus with maximum shear deformation and material damping, are captured rather closely by the formulation. In the constitutive model, the material degradation is affected by a function which depends on the Eulerian norm of the deviatoric strains. Volumetric strains are considered to be entirely elastic. The resultant analytical model simulates the bearing behavior rather realistically.

Since a base-isolated structure may have a highly nonlinear rubber bearing at its base and its foundation is embedded in a layered soil deposit, the suitable soil-structure interaction (SSI) analysis should be able to capture these important factors. Here, a three-step spring method[12] is adapted for the soil analysis. Briefly, it consists of three major steps. The first step calculates the foundation input motions (translation and rotation) from the site specific free-field motion. The calculation is based on the theory of elastic wave propagation in combination with the assumption that the motion is composed of the vertically propagating body waves. The second step evaluates the impedance functions for the embedded foundation. The third step is using the foundation input motion and impedance function as input to the SISEC code to perform the detailed SSI analysis.

Relative Response of Unisolated and Isolated Structures Under Horizontal Excitation

The finite-element model of a nuclear island is shown in Fig. 14. Two lumped-mass sticks are used to model the reactor containment and reactor building, respectively. In this model, the reactor containment is approximated by twelve (12) nodes interconnected by eleven (11) beam elements. The reactor building is discretized into eleven (11) nodes connected by ten (10) beam elements. The mass of the major components such as the reactor vessel is appropriately added to its associated nodes. Two calculations are performed dealing with unisolated and isolated plants, respectively. For the unisolated plant, one foundation mat is utilized. On the other hand, the isolated plant has two concrete foundation mats, and the isolators are placed between these two mats. The design fundamental frequency of the isolators is 0.50 Hz.

For calculation of the base-isolation structure, certain modeling techniques are required. In this calculation, beam elements are used for the super-structures. The isolators are modeled by two spring elements, one linear spring for simulating the large vertical stiffness and one nonlinear viscoelastic spring for modeling the relatively low stiffness in the horizontal direction. Thus, the vertical load-carrying capacity and necessary horizontal flexibility are appropriately modeled. The input parameters to the horizontal nonlinear spring using the viscoelastic constitutive model were based on experimental data of 1/4-scale PRISM-type bearings[13] and have the values:

$G_0 = 250$, $G_\infty = 55$, $\nu = 0.35$, $\alpha = 0.10$, $\beta = 0.30$, $C = 0.55$.

The area of the full-size PRISM bearing is 2124 in^2. A total of six hundred bearings is assumed for this illustration. For simplification of the analysis, only one composite isolator is used. This isolator represents the global effect of the estimated 600 isolators required for the frequency of 0.50 Hz. The free-

field artificial input acceleration history and its Fast Fourier Transform (FFT) shown in Fig. 15 is used for the numerical analyses which has a zero-per acceleration (ZPA) of 0.20 g.

To study the relative merits of the base-isolation system, the horizontal acceleration spectra at Node 1 (basemat), 23 (top of containment) and 43 (top of reactor building) for both the unisolated and isolated plants are given in Figs. 16 through 18. The advantage of isolation system in reducing the spectra accelerations of structures, as well as in lowering their response frequencies far below those frequency levels that contain most of the damage energy of earthquakes are very evident. For instance, for structures and equipment located on the top of the reactor building (see Fig. 18) whose fundamental frequencies are between 2.0 to 8.0 Hz, the acceleration transmitted in the isolated plant is at least seven times smaller than that of the unisolated structure. In other words, by using the high damping elastomeric bearings the superstructure is basically decoupled from the ground motion during the earthquake.

Figure 19 depicts the force-displacement hysteresis loop plots of the composite bearing. The maximum horizontal displacement is about 3.68 in.

Acknowledgements

This work was performed under the auspices of the U. S. Department of Energy, Office of Technology Support programs, under contract W-31-109-Eng-38.

References

1. R.F. Kulak and C. Fiala, "NEPTUNE: A System of Finite Element Programs for Three-Dimensional Nonlinear Analysis," Nucl. Engrg. Design, 106, 47-68 (1988).

2. C.Y. Wang, Y. Tang, R.A. Uras, A.H. Marchertas, Y.W. Chang, and R.W. Seidensticker, "Seismic Response Analysis of Base Isolated Structures with High Damping Elastomeric Bearings," in Seismic Engineering - 1991, 1991 ASME Pressure Vessel and Piping Conf., 15-22, San Diego, California (June 23-27, 1991).

3. C.Y. Wang, Y. Tang, and A.H. Marchertas, "System Response Analyses of Base-Isolated Structures to Earthquake Ground Motions," Trans. SMiRT-11 Conf., Tokyo, Japan, paper K26/6, to appear (Aug. 18-23, 1991).

4. M. Mooney, "A Theory of Elastic Deformation," J. Appl. Physics, 11, 582 (1940).

5. P.J. Blatz and W.L. Ko, "Application of Finite Elastic Theory to the Deformation of Rubber Materials," Trans. Soc. Rheology, VI, 223-251 (1962).

6. P.A.J. van den Bogert and R. de Borst, "Constitutive Aspects and Finite Element Analysis of 3D Rubber Specimens in Compression and Shear," Proc. Third Int. Conf. Numerical Methods in Engineering: Theory and Applications (NUMETA90) (Eds. G.N. Pande and J. Middleton), Elsevier Applied Science, London-New York, 870-877 (1990).

7. R.W. Ogden, "Large Deformation Isotropic Elasticity: On the Correlation of Theory and Experiment for Incompressible Rubberlike Solids," Proc. R. Soc. Lond. A., 326 (1972).

8. C.G. Koh and J.M. Kelly, "Fractional Derivative Representation of Seismic Response of Base-Isolated Models: Theory and Experiments," UCB/SESM 85/07, University of California at Berkeley (1985).

9. T.C. Simo and F.L. Taylor, "A Three-Dimensional Finite Deformation Viscoelastic Model Accounting for Damage Effects," Report No. UCB/SESM/85-02, SESM, Univ. of California, Berkeley (1985).

10. R.F. Kulak and C.Y. Wang, "Design and Analysis of Seismically Isolated Structures," Proc. 1st Intl. Seminar on Seismic Base Isolation for Nuclear Power Facilities, CONF-8908221, 341-368, San Francisco, California (Aug. 21-22, 1989).

11. M.J. Kim, A. Gupta, and A.H. Marchertas, "Implementation of a 3-D Viscoelastic Material Model," Report NIU/ME 89/01, Northern Illinois University (Sept. 1990).

12. E. Kausel, R.V. Whitman, J.P. Morray, and F. Elsabee, "The Spring Method for Embedded Foundations," Nucl. Engrg. Design 48, 377-392 (1978).

13. F.F. Tajirian and T.M. Kelly, "Testing of Seismic Isolation Bearings for Advanced Liquid Metal Reactor Prism," in Seismic, Shock, and Vibration Isolation - 1988, H. Chung and N. Mostaghel, eds., ASME Publication, PVP - Vol. 147 (1988).

Table 1. Difference in secant modulus between the up sequence and down sequence

Strain (%)	Up	Down	Average
5	343	312	327
10	266	248	257
20	207	196	201
50	146	140	143
100	116	112	114
150	121	121	121

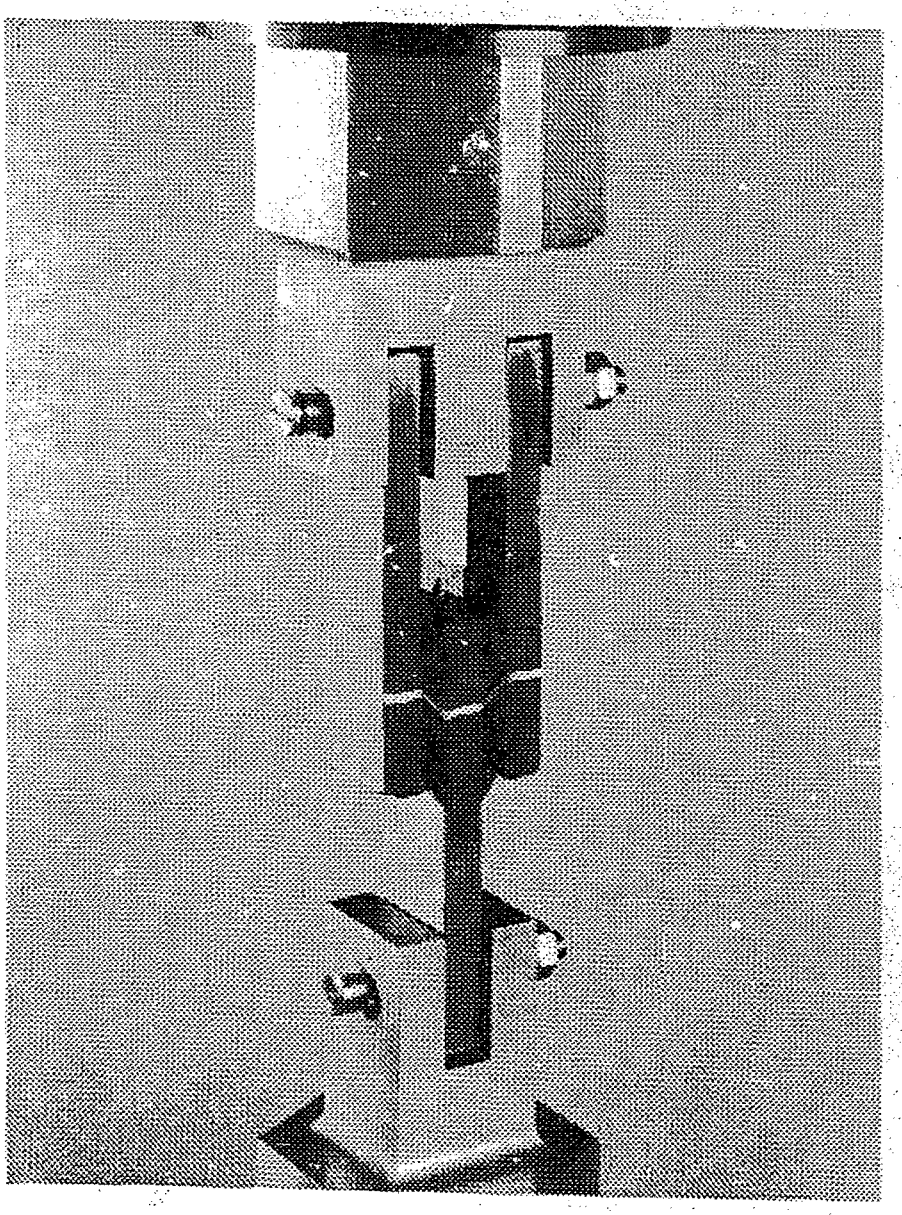

Fig. 1. Three-Bar Shear Specimen

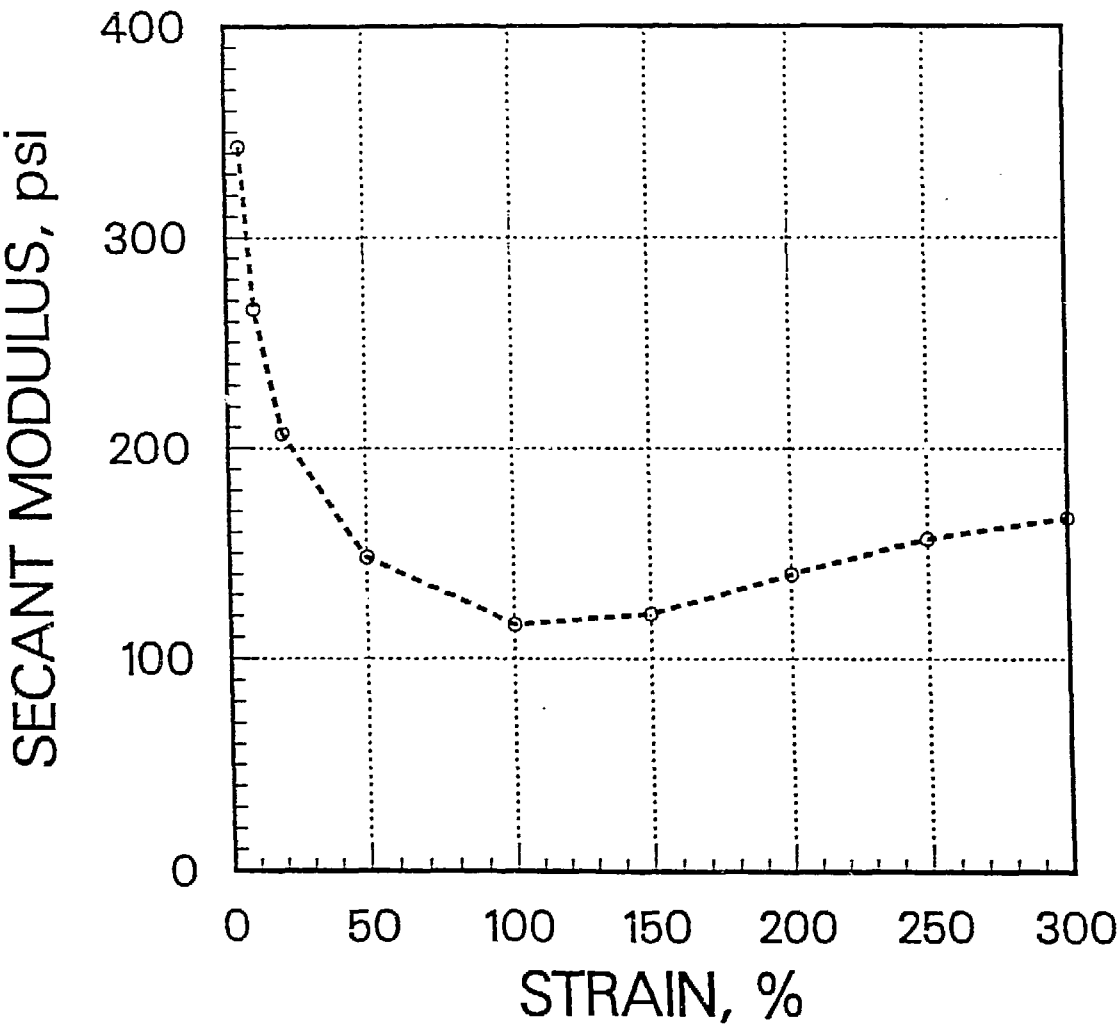

Fig. 2. Variation in Stiffness with Shear Strain

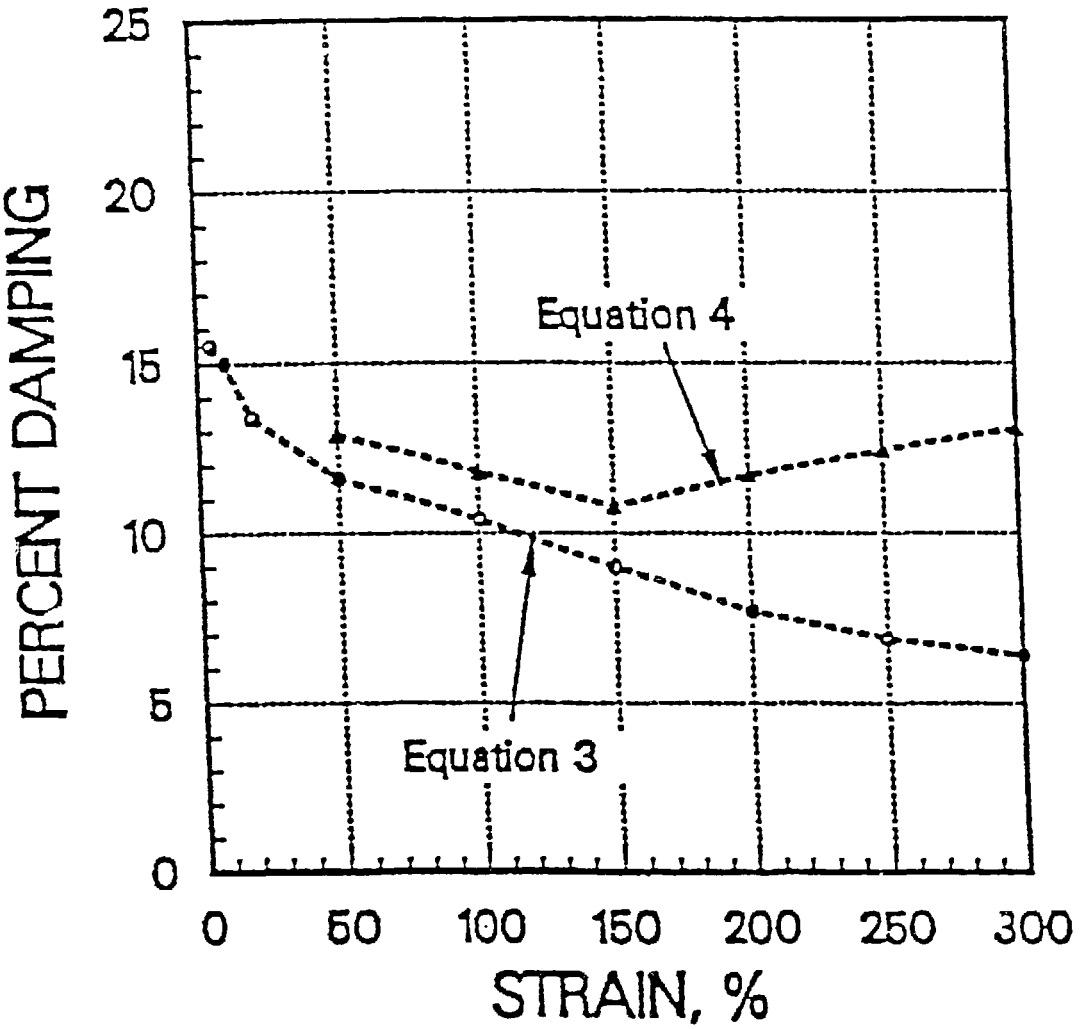

Fig. 3. Variation in Damping with Shear Strain

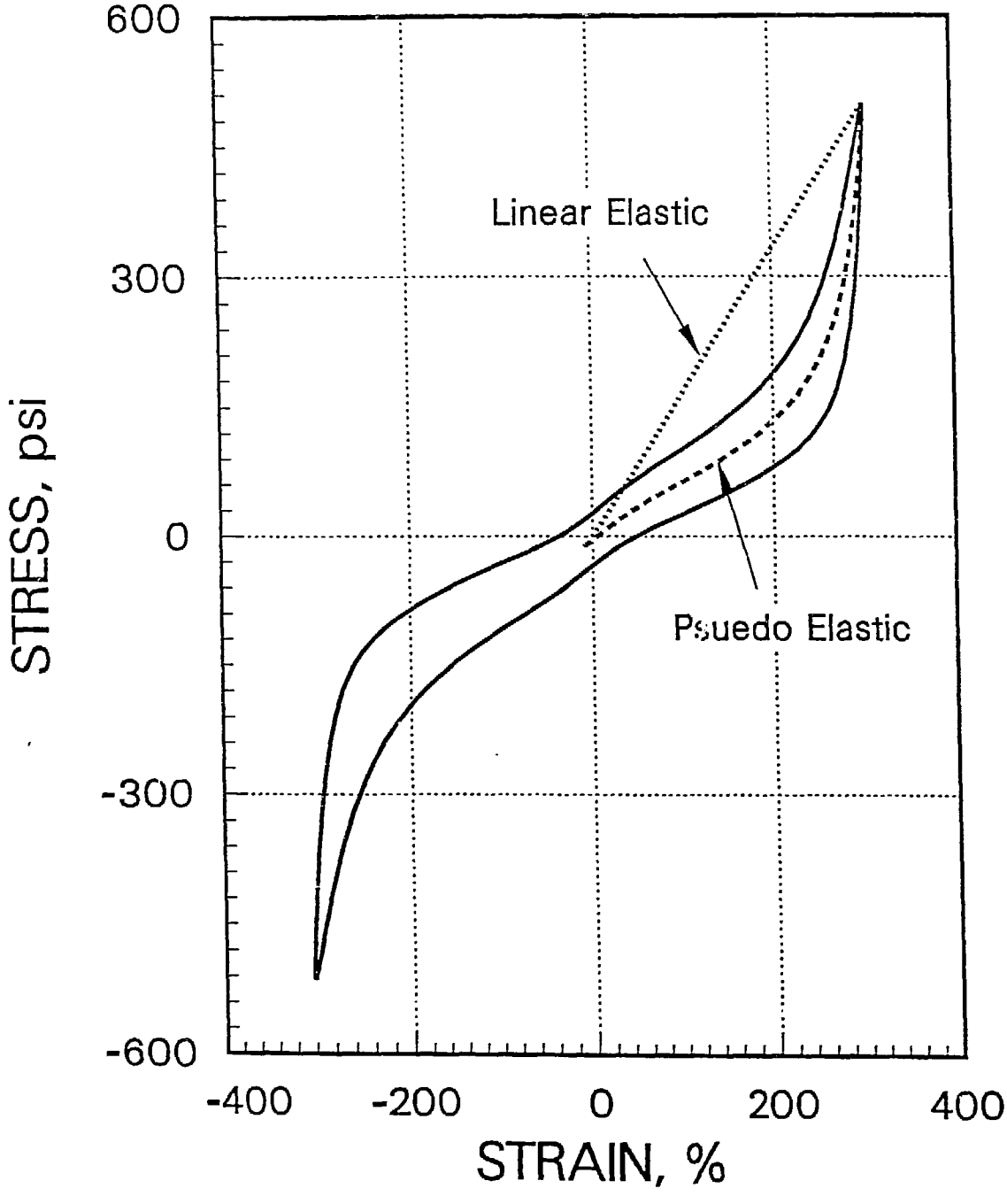

Fig. 4. Hysteresis Loop for 300 Percent Shear Strain

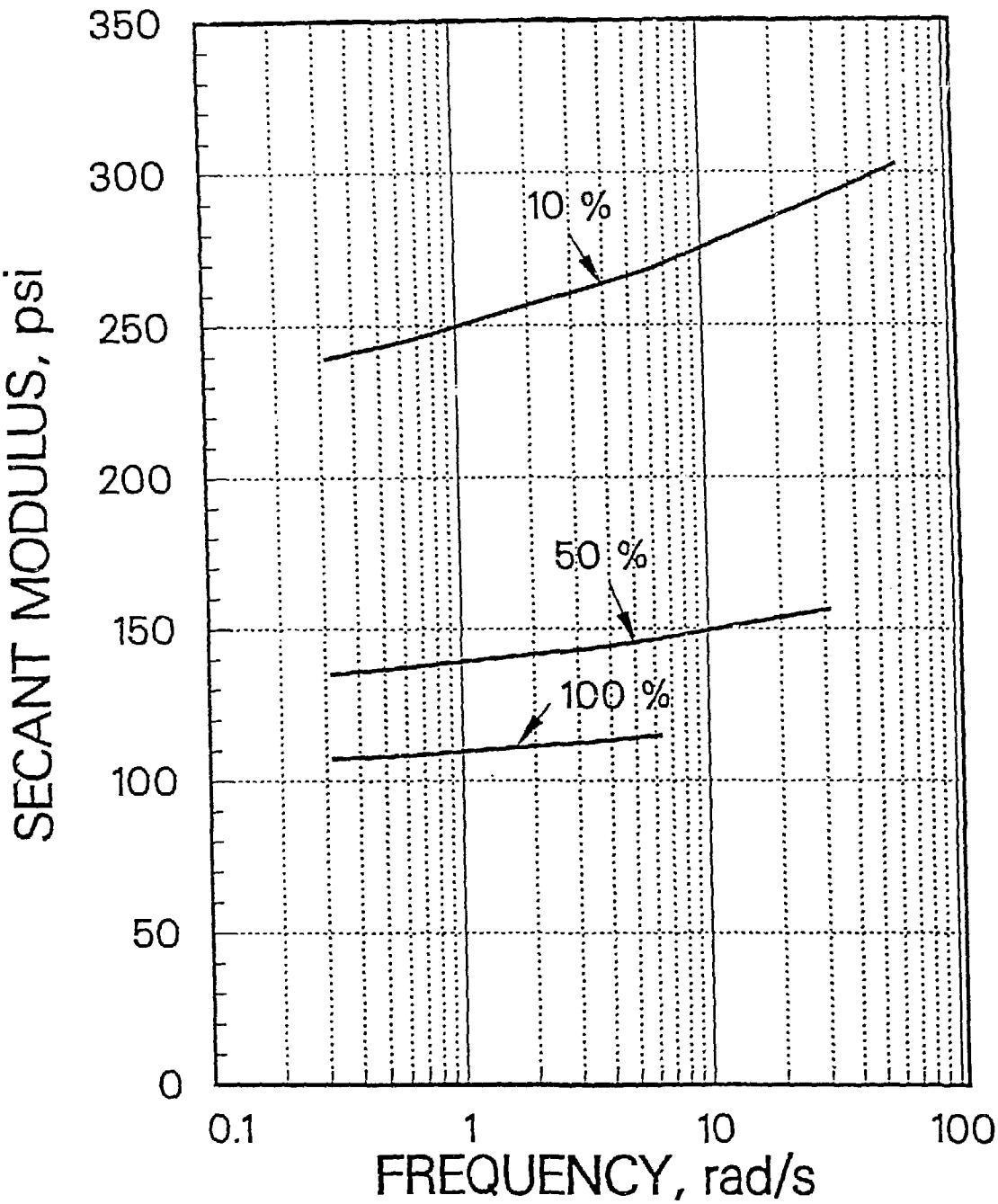

Fig. 5. Variation in Stiffness with Frequency and Strain Level

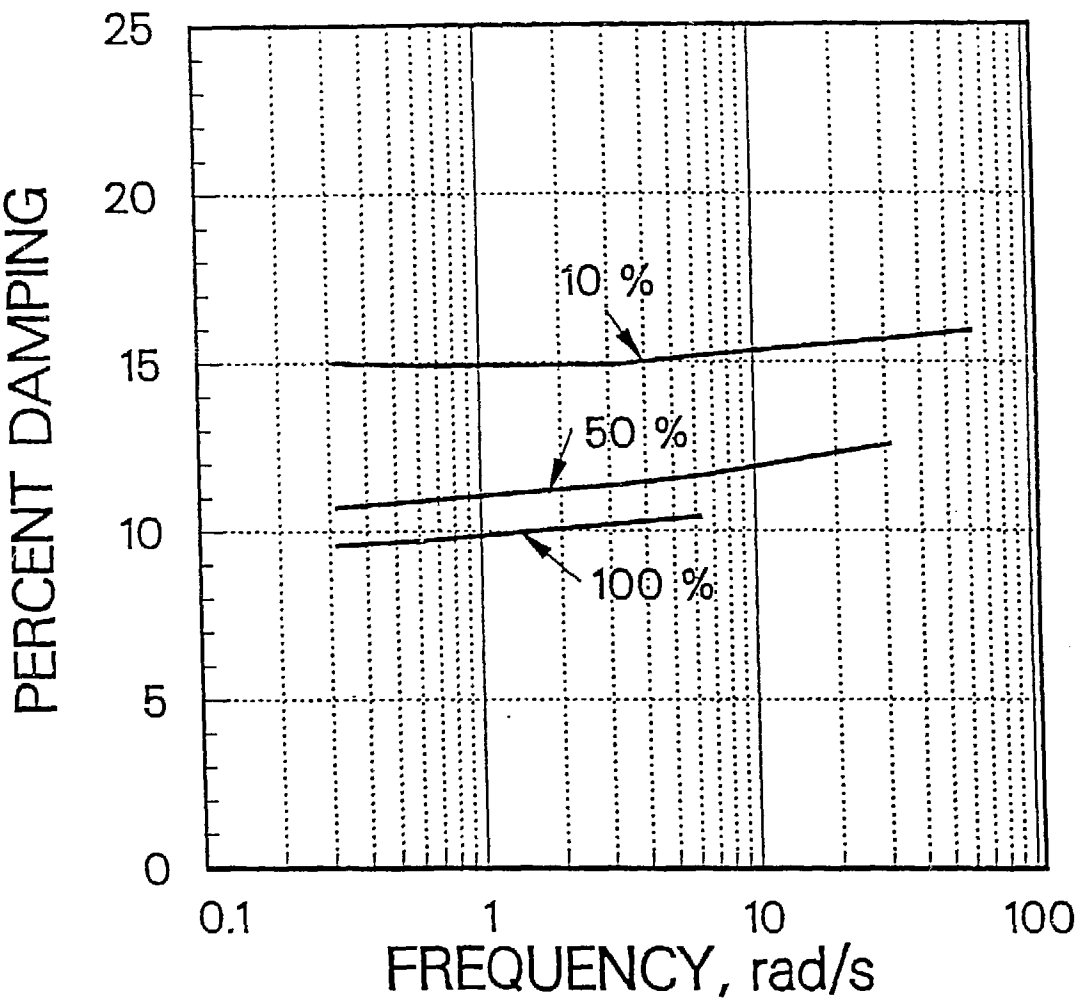

Fig. 6. Variation in Damping with Frequency and Strain Level

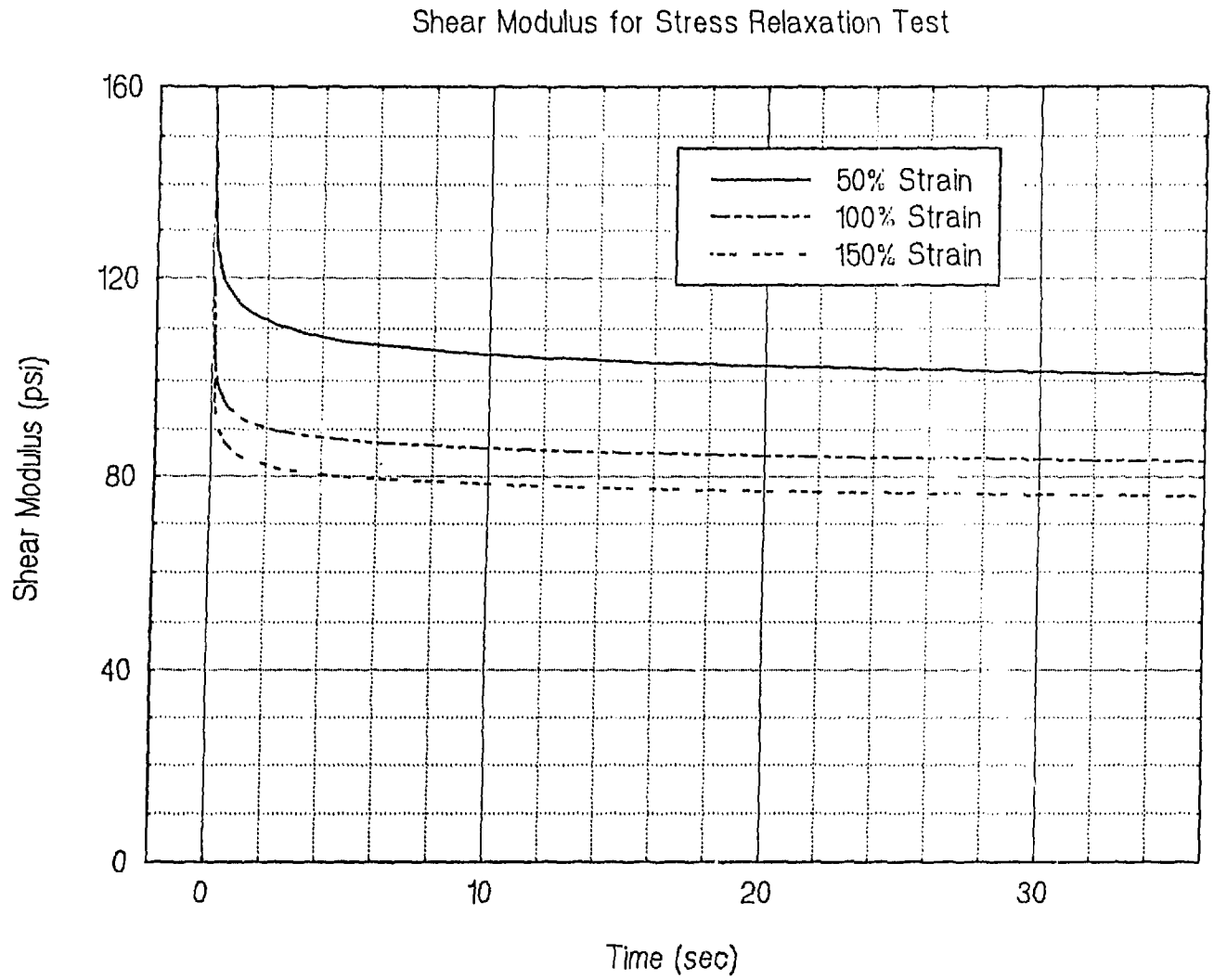

Fig. 7. Stress Relaxation at 50, 100, and 150 Percent Shear Strain

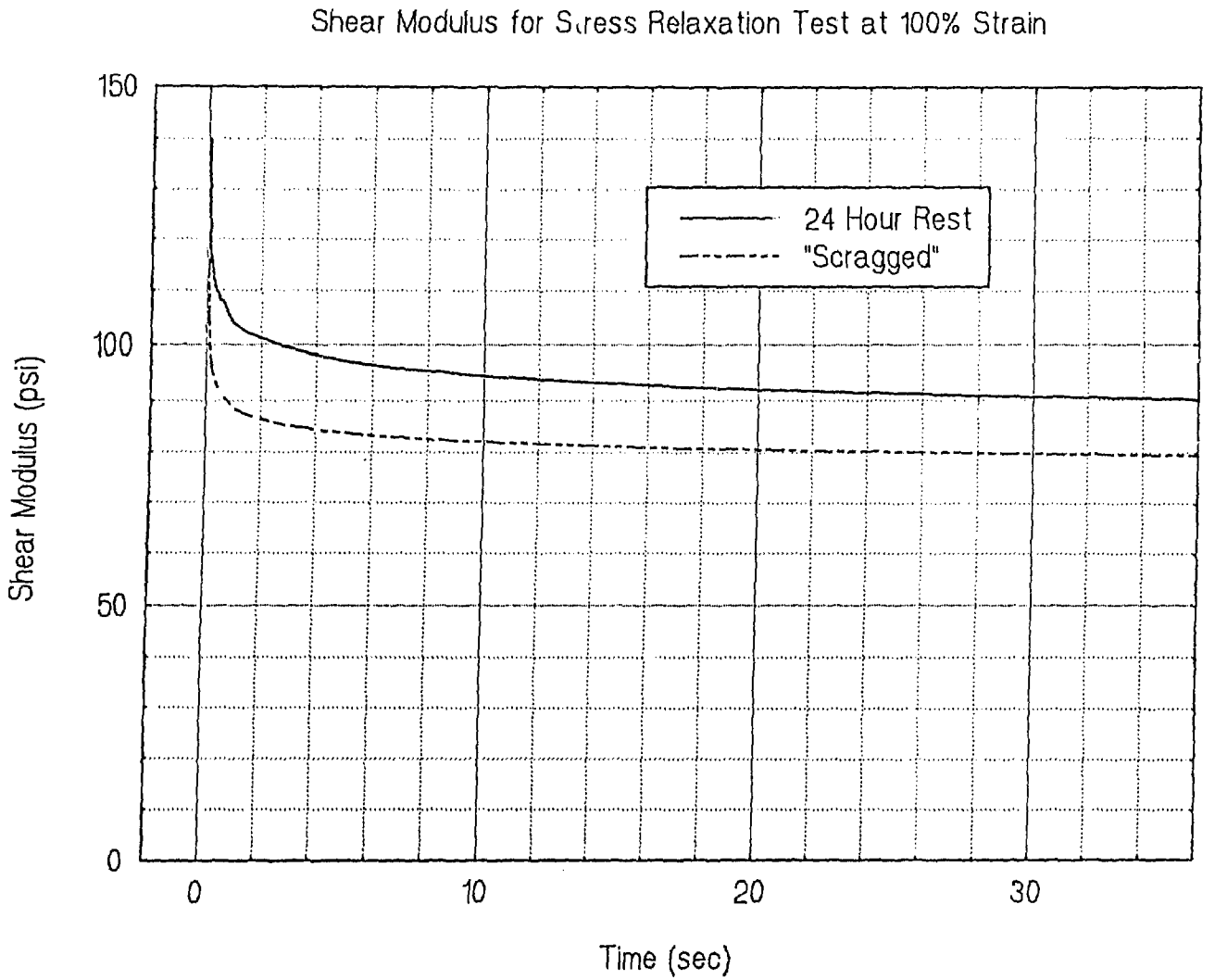

Fig. 8. Effect of Scragging on Stress Relaxation at 100 Percent Shear Strain

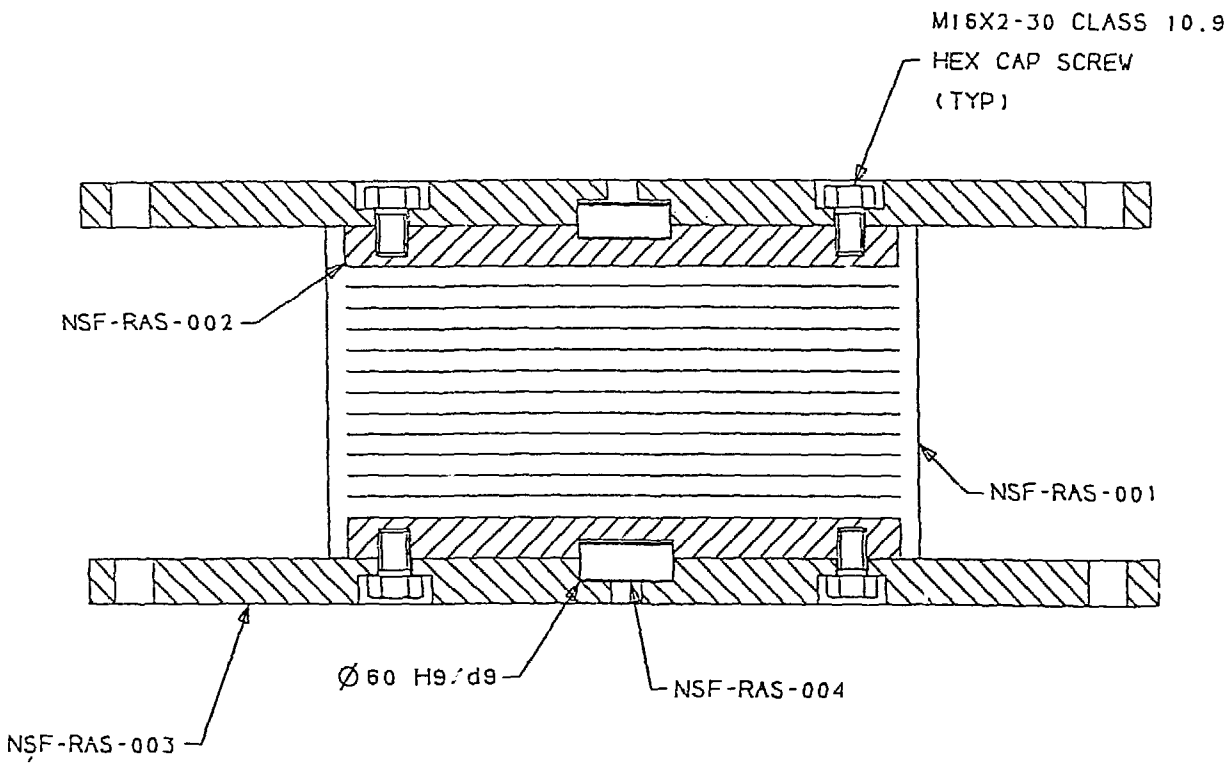

Fig. 9. Assembly Drawing for a Typical Steel Laminated Isolation Bearing

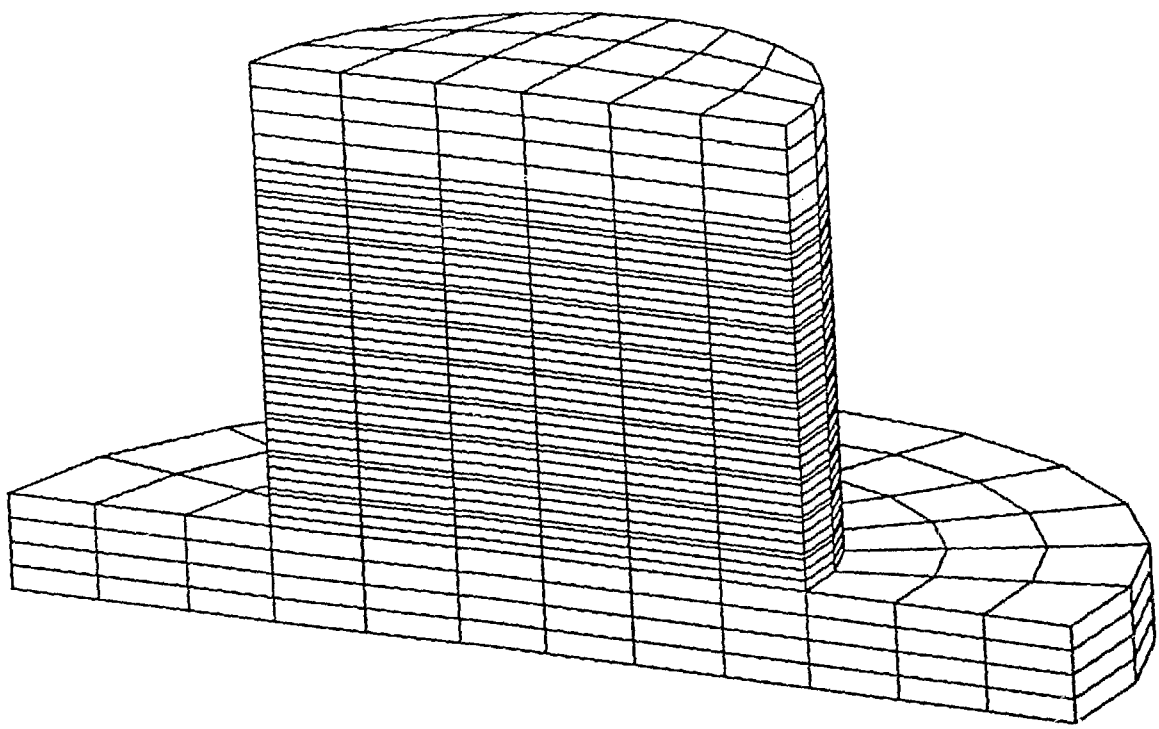

Fig. 10. Partially Generated Finite Element Model for a Bearing

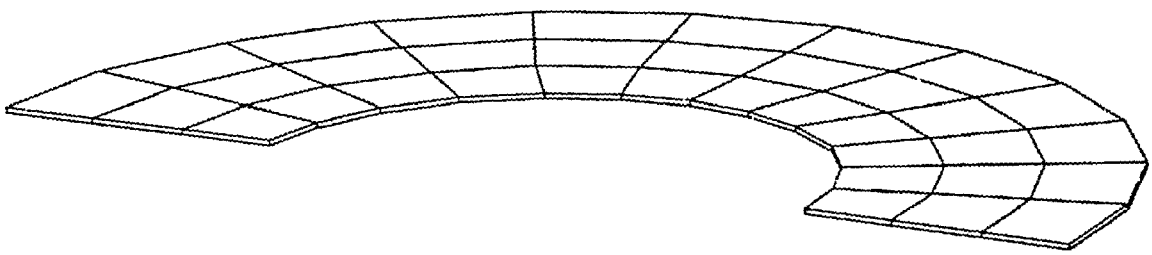

(b)

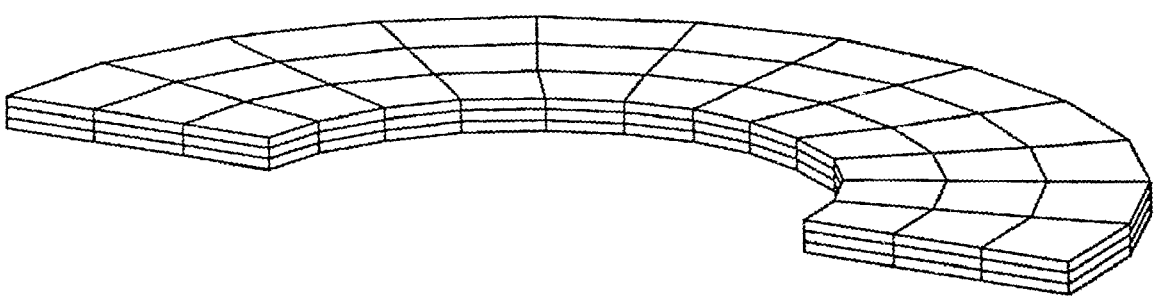

(a)

Fig. 11. (a) Single Outer Layer of Rubber - Three Elements Thru Thickness; (b) Single Outer Layer of Shim

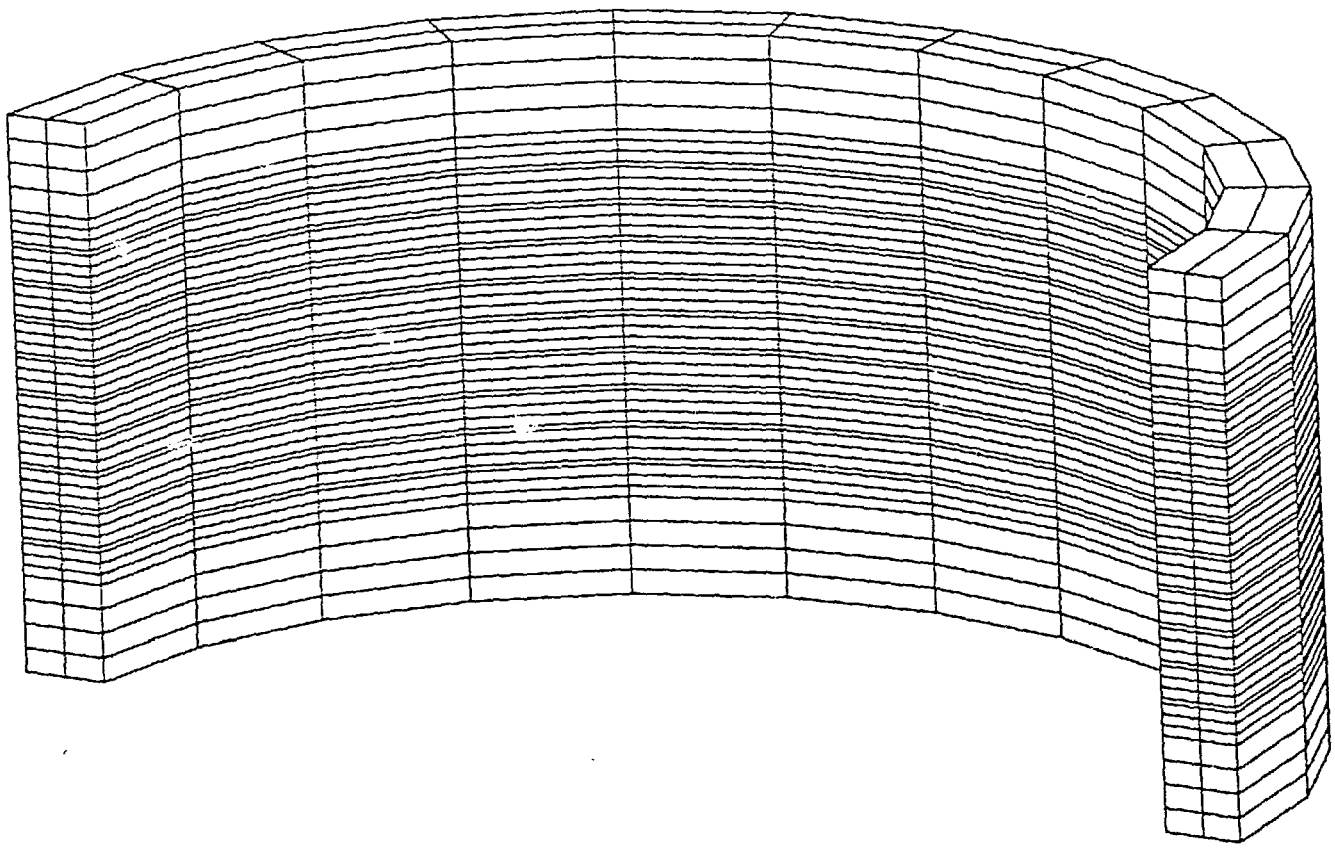

Fig. 12. Outer Rubber Cover Layer for the Entire Bearing

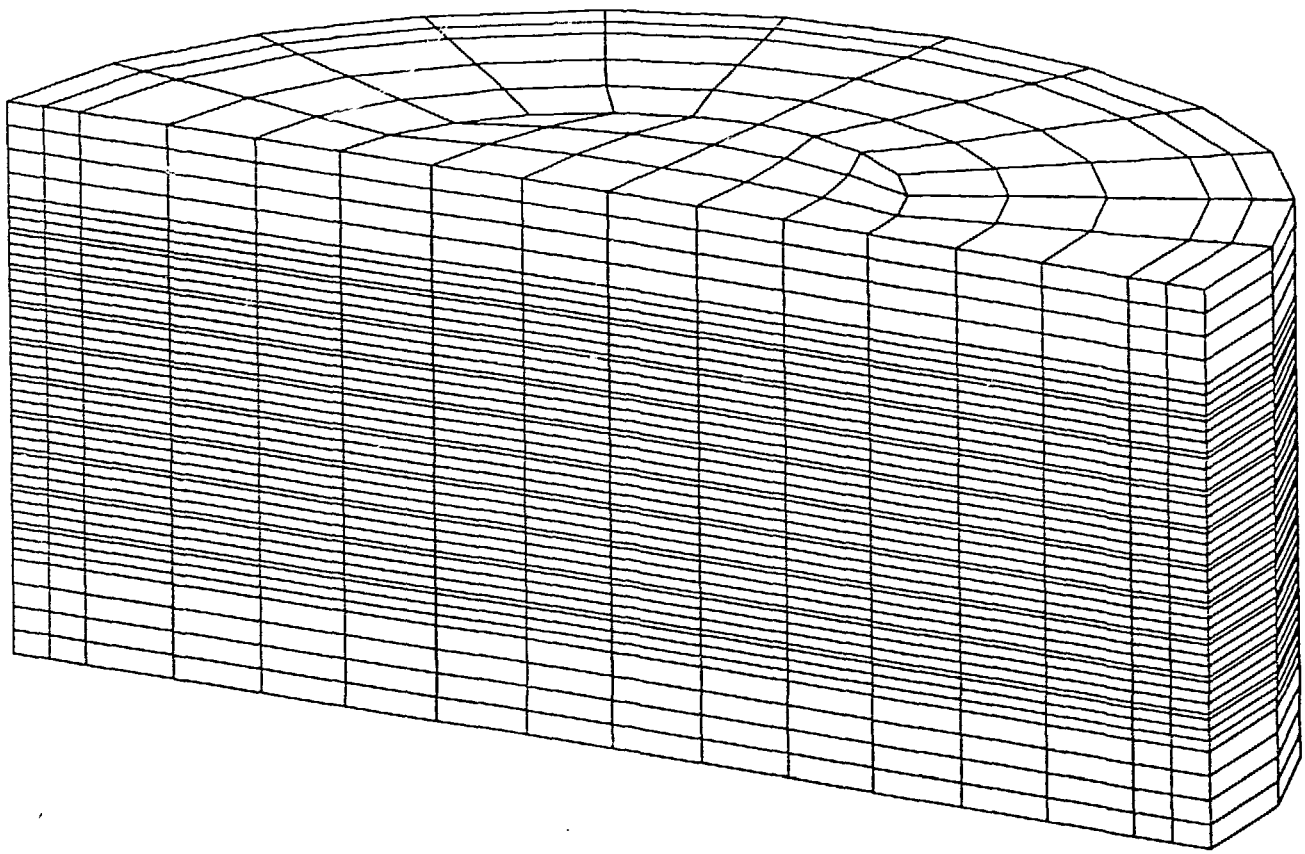

Fig. 13. Completed Finite Element Model for a Steel Laminated Isolation Bearing

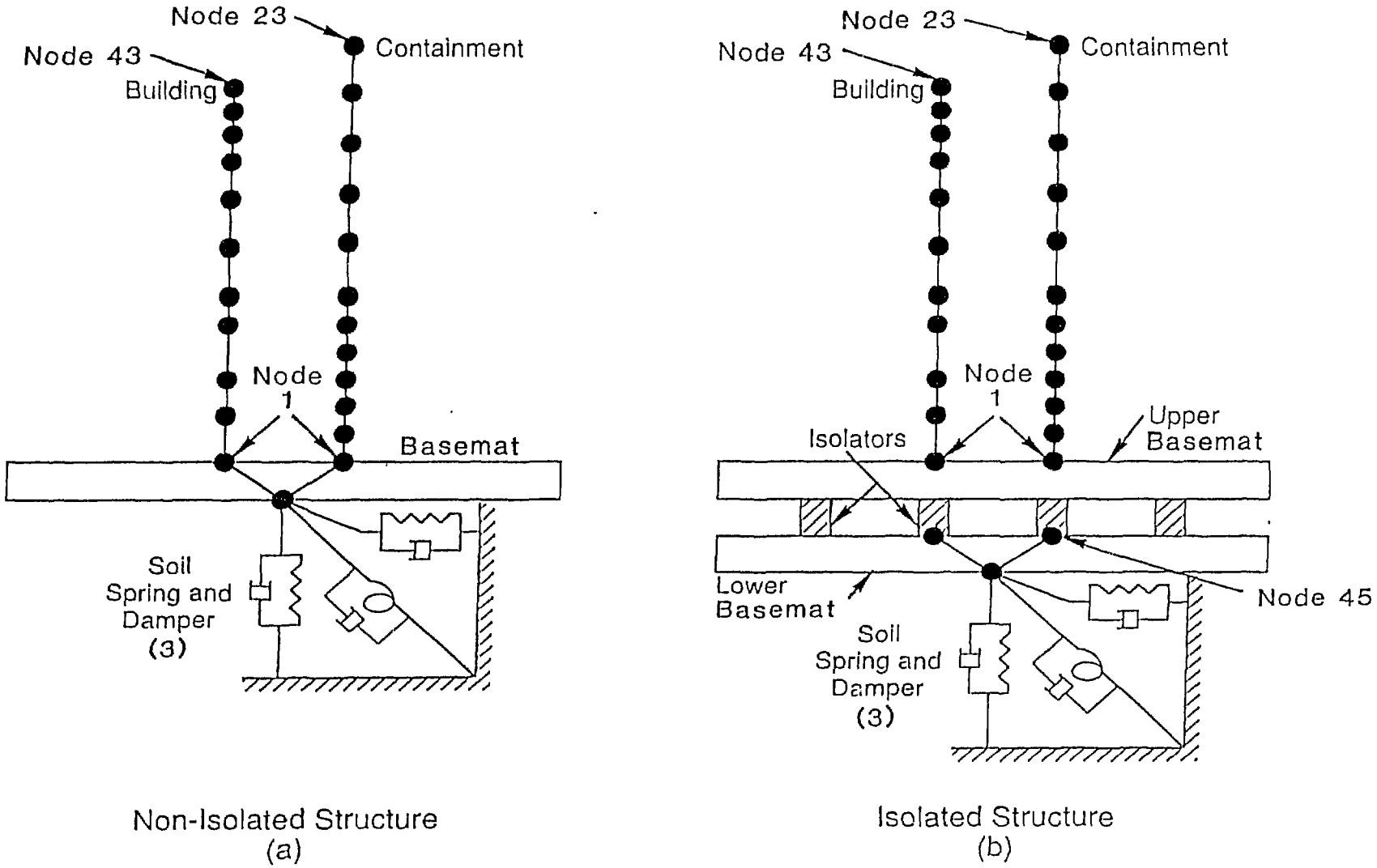

Fig. 14. Finite Element Model of a Nuclear Island

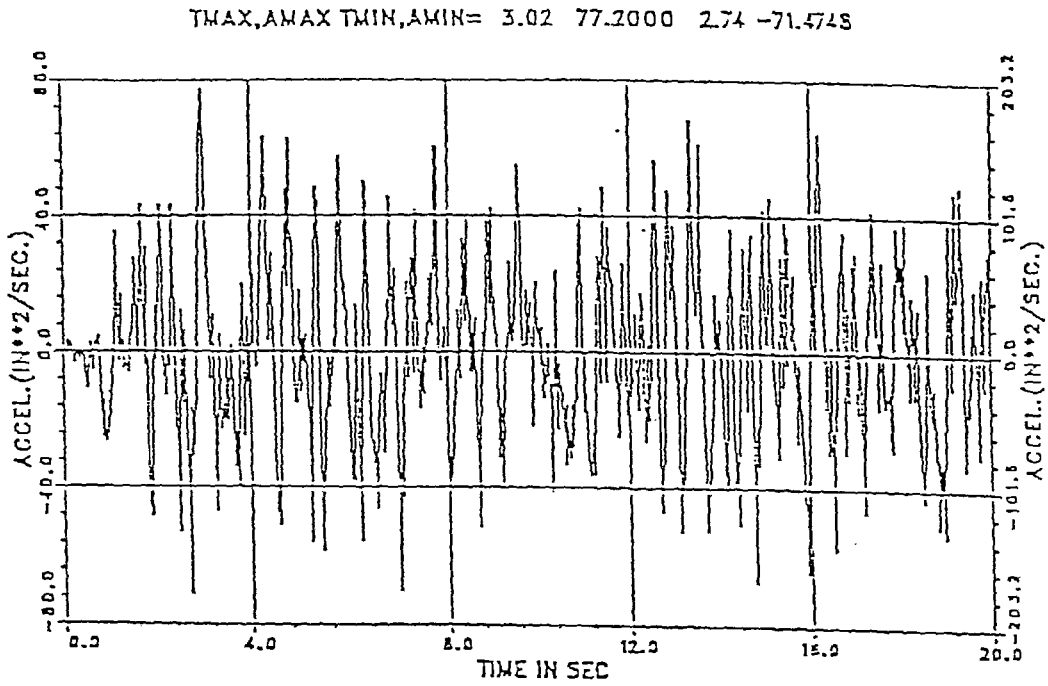

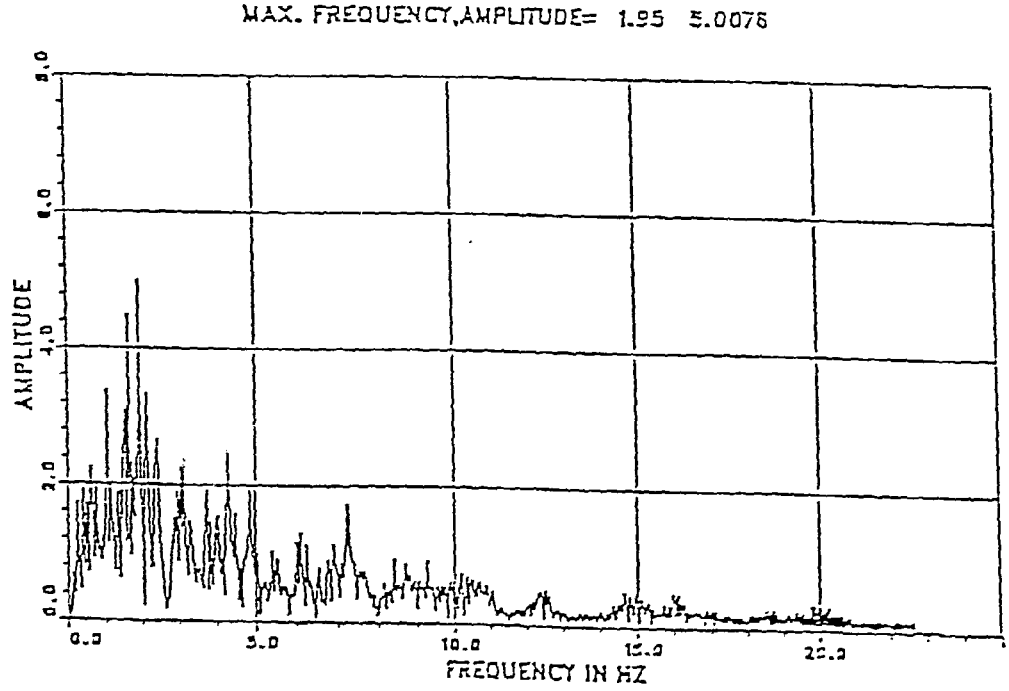

Fig. 15. The Input Free Field Artificial Acceleration History for Simulating the Horizontal Excitation

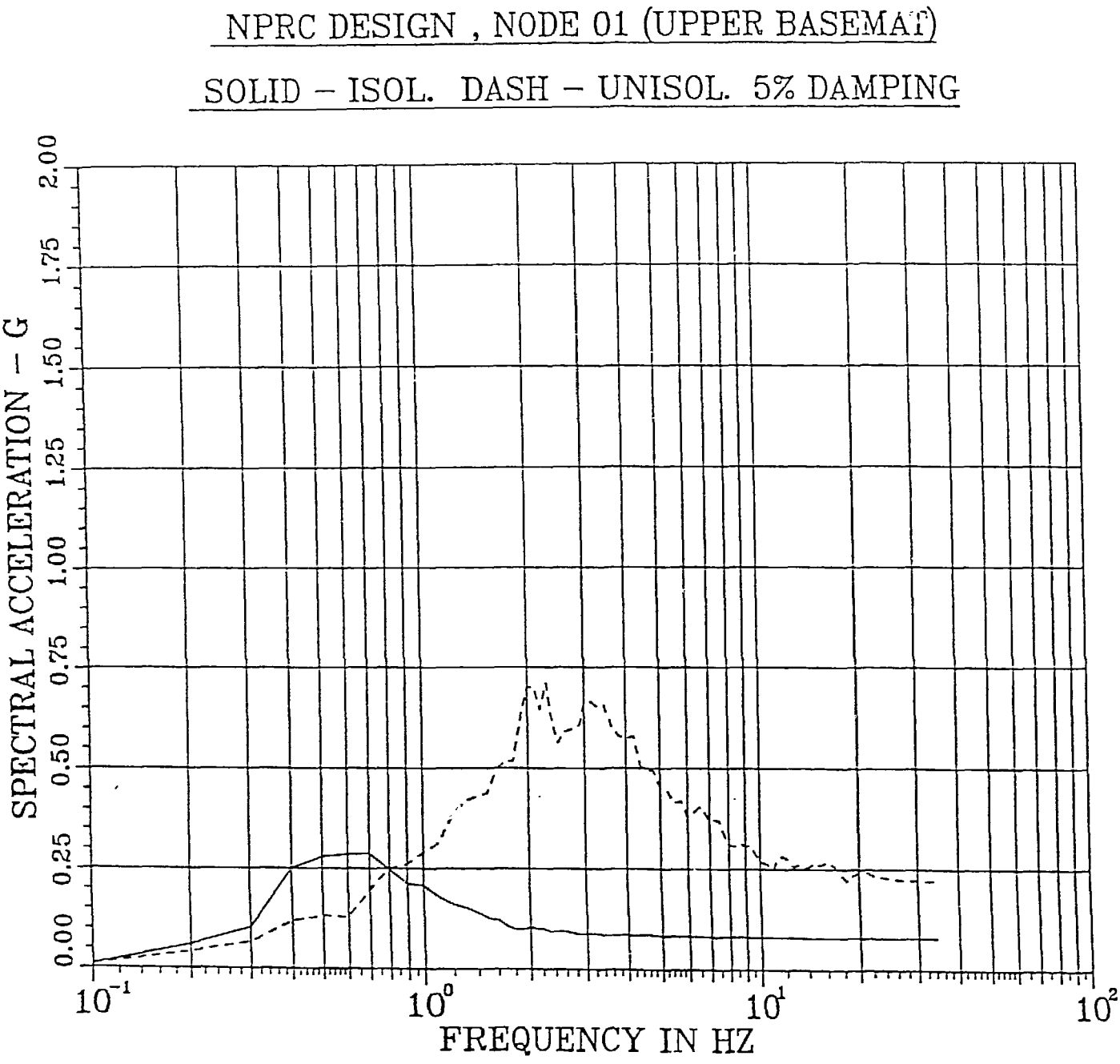

Fig. 16. Horizontal Acceleration Spectra for Upper Basemat (Node 1)

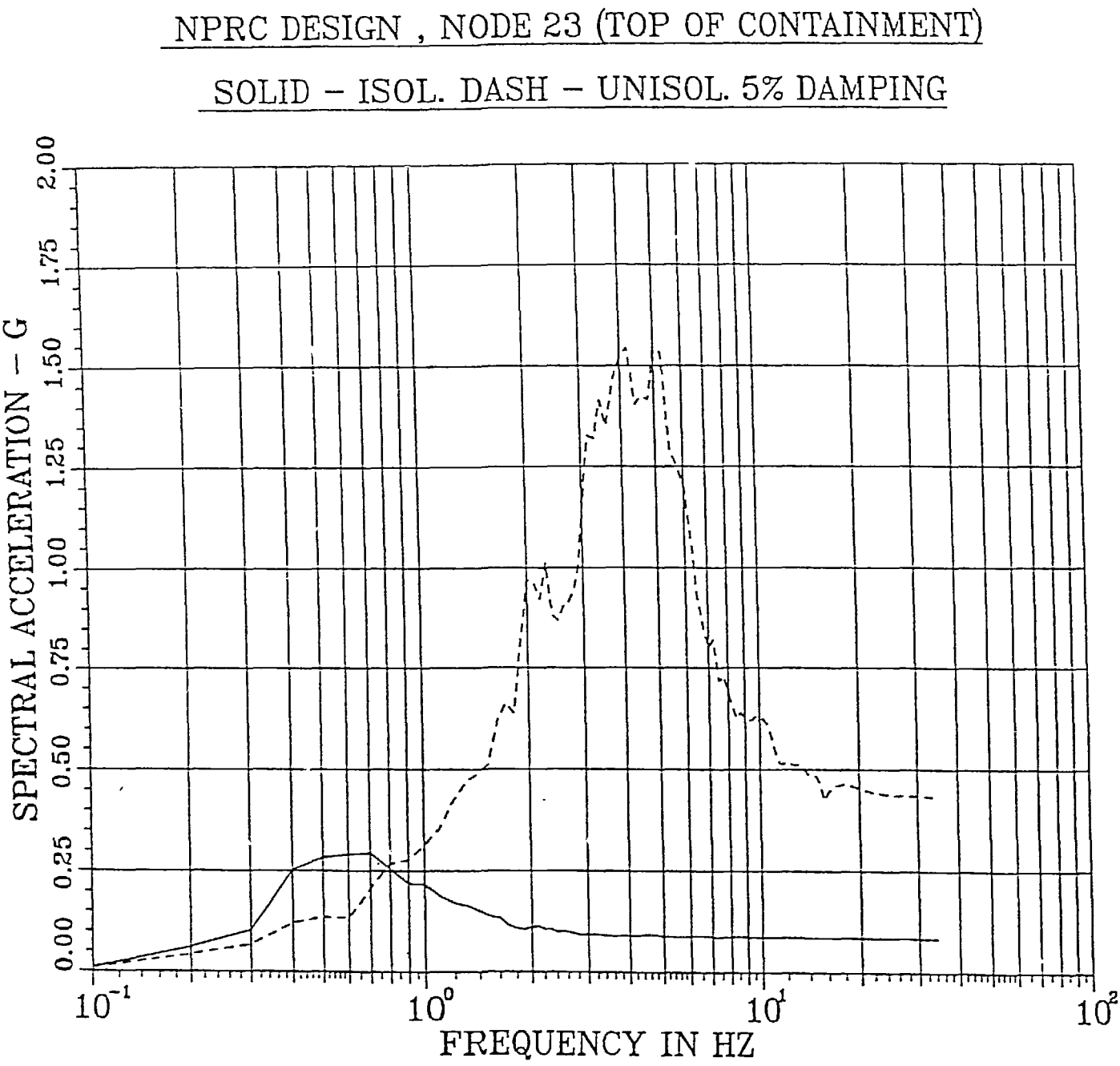

Fig. 17. Horizontal Acceleration Spectra for Top of Containment (Node 23)

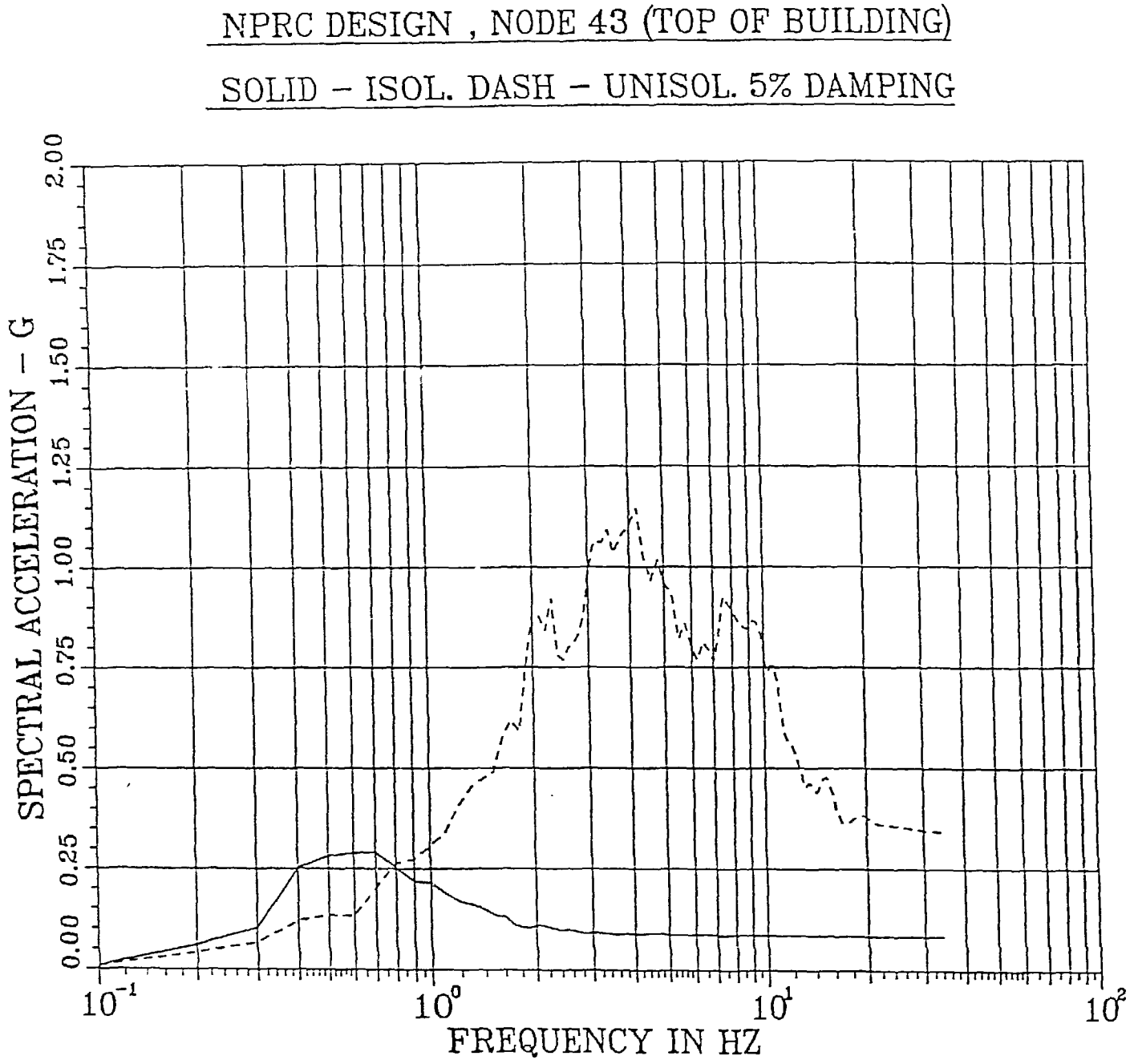

Fig. 18. Horizontal Acceleration Spectra for Top of the Building (Node 43)

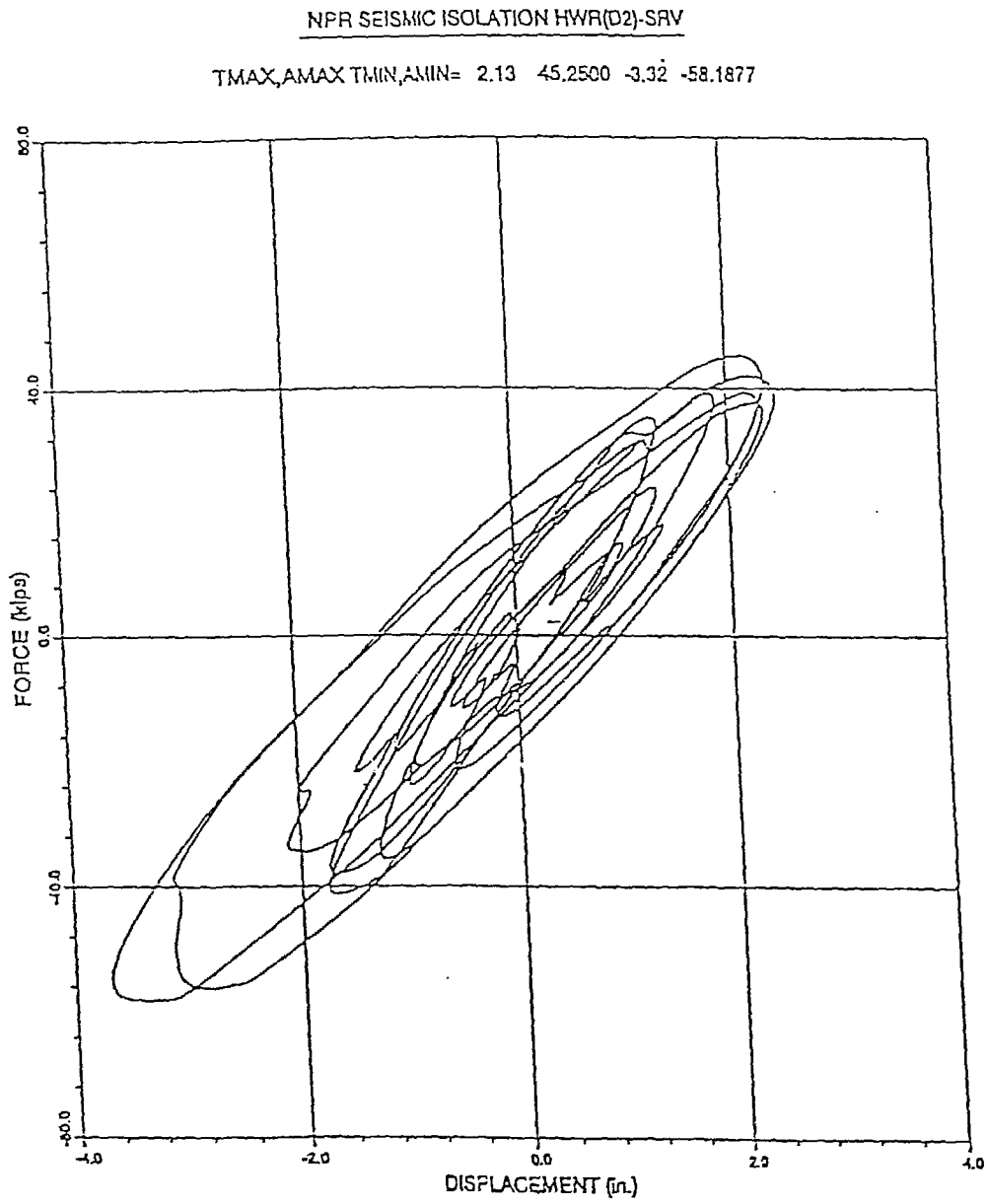

Fig. 19. Force-Displacement Hysteresis Loops of the Composite Bearing